

# *Ab initio* description of magnetic properties of spin-glass pyrochlore NaSrMn<sub>2</sub>F<sub>7</sub>

Mohammad Amirabbasi\*

*Department of Physics, Isfahan University of Technology (IUT), Isfahan 84156-83111, Iran and  
Faculty of Physics, University Duisburg-Essen, 47057 Duisburg, Germany*

(Dated: July 27, 2022)

The magnetic and critical properties of manganese pyrochlore fluoride NaSrMn<sub>2</sub>F<sub>7</sub> have been determined which exhibits a glass transition due to charge disorder. Spin-Hamiltonian calculations show that only the Heisenberg exchange plays a significant role in determining the magnetic order of the ground state. The Monte Carlo simulation detects that without considering weak bond disorder ( $\delta J$ ), no phase transition is observed at temperature variation of specific heat. The  $\delta J=0.34$  meV has been calculated by using Monte Carlo simulations in such a way that the obtained spin freezing temperature will be equal to the experimental one. The microscopic calculation of  $\delta J$  within DFT for different Na/Sr distributions proves that  $\delta J$  should be around 0.31 meV. The (h0l) planes density plot of elastic neutron scattering structure function at low-temperature shows that the ground state has a degenerate manifold due to the different numbers of short-range degrees of freedom. The data collapsing of specific heat for different lattice sizes by using finite-size scaling theory confirms that the obtained freezing temperature by considering  $\delta J=0.34$  meV is in good agreement with experimental measurements.

PACS numbers: 71.15.Mb, 75.40.Mg, 75.10.Hk, 75.30.Gw

## I. INTRODUCTION

Spin-glass (SG) is a type of magnetic phase in which the spatial arrangement of spins at low-temperatures is completely random<sup>1-4</sup>. The presence of frustration (co-existing and competing ferromagnetic and antiferromagnetic interactions) and randomness (such as chemical disorders or weak bond disorders) are essential for glass formation<sup>1,2,6</sup>. These materials undergo a second-order phase transition which makes the study of SG materials attractive to scientists<sup>6</sup>. Experimental evidences to detect such a phase are the bifurcation of the field cooled (FC) and zero field cooled (ZFC) of DC susceptibility, the frequency dependence of AC susceptibility, no magnetic saturation even at low-temperature and high magnetic field and diffusive peaks inelastic neutron scattering pattern<sup>1,3,7</sup>. In recent years, some geometrically frustrated pyrochlores have shown the SG phase<sup>8,9</sup>. These materials are composed of a network of corner-sharing tetrahedra<sup>10,11</sup>. If the exchange interaction between the nearest neighbor is antiferromagnetic, the system fails to reach the ground state with a global minimum. This condition is called geometric frustration<sup>10-13</sup>. Despite many studies and research, there are still many questions about what is the truly thermodynamic SG transition<sup>2</sup>. Determination of the ground state of classical Heisenberg antiferromagnetic SG pyrochlores in which only Heisenberg interactions play a key role can be a good candidate to answer these questions.

In 1997, with the discovery of the spin-ice phase in Ho<sub>2</sub>Ti<sub>2</sub>O<sub>7</sub><sup>14</sup>, a study on the magnetic properties of oxide pyrochlores increased<sup>15-21</sup>. One of the main problems in the study of these materials is the difficult conditions of their crystal growth. As a consequence, the availability of large crystal pyrochlores in large sizes has made it impossible. There is no such problem for py-

rochlore fluoride with general chemical formula A<sub>2</sub>B<sub>2</sub>F<sub>7</sub> in which Na<sup>1+</sup>/Sr<sup>2+</sup>(Ca<sup>2+</sup>) atoms occupy A-site position randomly and magnetic atoms such as Mn<sup>2+</sup>, Fe<sup>2+</sup>, Co<sup>2+</sup> and Ni<sup>2+</sup> occupy B-site<sup>5,22-24</sup>. The result of this random occupation is the presence of the  $\delta J$  (difference in the bond angle between the magnetic ions). Therefore, all of these materials exhibit SG properties at low-temperatures<sup>9,53</sup>. In this paper, I intend to investigate the magnetic and critical properties of NaSrMn<sub>2</sub>F<sub>7</sub> which has the largest spin moment among the pyrochlore fluoride by first-principle methods in the framework of DFT and Monte Carlo (MC) simulation. In this material, the Mn<sup>2+</sup> terminates in 3d<sup>5</sup>. Therefore, S=5/2 and the orbital moment has a small contribution to the effective moment (6.25  $\mu_B$ /Mn<sup>5</sup>). The absence of orbital moment and its associated complexities make this material a suitable candidate to study the effect of bond weak disorder in the phase transition of SG ground state.

The lattice of the NaSrMn<sub>2</sub>F<sub>7</sub> consists of two separate sublattices with corner-shared tetrahedra (Fig. 1). In one sublattice, the Na<sup>1+</sup>/Sr<sup>2+</sup> ions and in the other the magnetic ion (Mn<sup>2+</sup>) sit on the vertices of each tetrahedra. The space group of this pyrochlore is Fd-3m (No. 227). Accordingly, the Na<sup>1+</sup>/Sr<sup>2+</sup>, Mn<sup>2+</sup> and F<sup>1-</sup> occupy the 16d (0.5, 0.5, 0.5), the 16c (0, 0, 0), 48f ( $x$ , 1/8, 1/8) and the 8b (3/8, 3/8, 3/8), respectively. The only variable parameter in this structure is the  $x$ -positional parameter. This parameter controls the bond angle (Mn-F-Mn) and bond length (Mn-F) which plays a decisive role in the magnetic properties. Experimental experiments show that this material is an insulator and shows a SG transition at 2.5 K<sup>5</sup>. The most important reason for SG transition can be attributed to the change in the bond angle due to the presence of charge disorder (Na<sup>1+</sup>/Sr<sup>2+</sup>) in the lattice<sup>5</sup>. The interaction between Mn<sup>2+</sup> ions is the superexchange mediated by F<sup>1-</sup>. This mechanism is di-

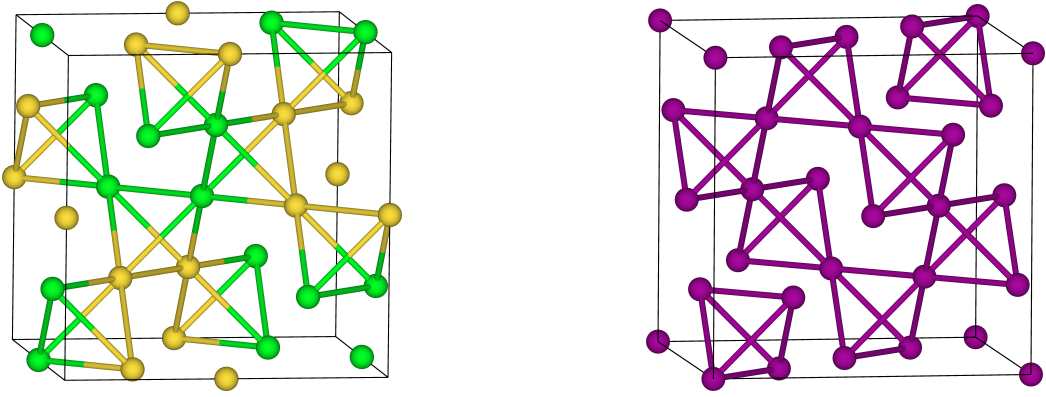


FIG. 1: (Color online) Crystal structure of SG pyrochlore  $\text{NaSrMn}_2\text{F}_7$  with corner-shared tetrahedrons for **(Left)** A-site (Na-Sr atoms) and **(right)** B-site (Mn atoms). Green, yellow and purple spheres are  $\text{Na}^{1+}$ ,  $\text{Sr}^{2+}$  and  $\text{Mn}^{2+}$ , respectively.  $x=0.3331$  is experimental value which is reported from the X-ray measurement<sup>5</sup>. The experimental lattice constant, bond length and bond angle in this material are 80.9 and 99.1 ( $^\circ$ ), 2.06( $\text{\AA}$ ) and 10.8012(3)( $\text{\AA}$ ), respectively<sup>5</sup>.

rectly related to the bond length and bond angle. The change in bond angle causes variations in exchange parameters. As a result, the ground state of the system takes SG order. The Curie-Weiss temperature ( $\theta_{\text{CW}}$ ) equals  $-89.72$  K which indicates the presence of strong antiferromagnetic interactions between magnetic ions<sup>5</sup>.

Microscopic examination of the exchange interactions in this material and its effect on the formation of the SG phase as well as the study of the critical properties seem interesting. This paper aims to determine magnetic and critical properties of  $\text{NaSrMn}_2\text{F}_7$  by constructing a spin Hamiltonian model. It includes various interactions such as the Heisenberg exchange parameters up to the third neighbor, the bi-quadratic, single-ion anisotropy (SIA) and Dzyaloshinskii-Moriya interactions (DMI) as obtained by the first-principle methods. By using this information, one can obtain the critical properties of this material, including transition temperature and spin correlation and elastic neutron scattering by the MC simulation. The current calculations show that only the  $J_1 + \delta J$  is important in determining the magnetic properties of this material, and the effect of other interactions is negligible. As a result, this material is considered as a simple model of SG and it can be a good candidate for further studies such as understanding the electron-electron correlation influence on magnetic ground state<sup>26</sup> especially in the SG phase, the effect of  $\delta J$  on thermal fluctuations and removing huge degeneracy<sup>53</sup> and what is the border between SG and liquid phase according to the strength of  $\delta J$ <sup>27-29</sup>.

The paper is structured as follows. In section II the details of the DFT and MC computational methods have been presented. Section III is devoted to deriving the spin Hamiltonian and the different aspects of exchange interactions in determination of magnetic ground state of  $\text{NaSrMn}_2\text{F}_7$  and in the following, the critical properties are discussed. Finally, In section IV a summary is given.

## II. COMPUTATIONAL METHODS

In this paper, the experimental lattice constant and  $x$ -positional parameter have been examined. One introduces the classical spin Hamiltonian ( $H$ ) to get magnetic properties of SG pyrochlore  $\text{NaSrMn}_2\text{F}_7$ :

$$H_{\text{spin}} = -\frac{1}{2} \sum_{i \neq j} J_{ij} (\vec{S}_i \cdot \vec{S}_j) + \frac{1}{2} B \sum_{\text{n.n}} (\vec{S}_i \cdot \vec{S}_j)^2 + \frac{1}{2} D \sum_{\text{n.n}} \hat{D}_{ij} \cdot (\vec{S}_i \times \vec{S}_j) + \frac{1}{2} \Delta \sum_i (\vec{S}_i \cdot \vec{d}_i)^2 \quad (1)$$

where  $\vec{S}_i$  denotes magnetic spins, vector  $\hat{D}_{ij}$  shows direction of DM which is determined by Moriya's rules<sup>30,31</sup> and vector  $\vec{d}_i$  is the single-ion easy-axis direction at each site  $i$ . According to Moriya's rules, if the mirror planes join two sites and the middle point of the opposite bond then the DM vectors should be perpendicular to the mirror plane<sup>30,31</sup>. It should be noted that in this model  $|\vec{S}|=1$ . Different terms of spin Hamiltonian express different types of exchange interactions without (isotropic terms) and with (anisotropic terms) considering spin-orbit coupling (SOC). Isotropic terms,  $J_{ij}$  and  $B$  are Heisenberg and bi-quadratic coupling, respectively. Heisenberg interaction decreases rapidly with distance because the  $\text{NaSrMn}_2\text{F}_7$  is an insulator. Therefore, Heisenberg terms are calculated up to the third nearest neighbor ( $J_1, J_2$  and  $J_{3a}$ ). To this end, one has to regard the conventional unit-cell (88 atoms) with  $4 \times 4 \times 4$  optimized Monkhorst-Pack k-point mesh. Then,  $J_1, J_2$  and  $J_{3a}$  values can be obtained by calculating the total energy of different collinear spin configurations and mapping them to the Heisenberg model (Fig. 2). There are two possible third nearest neighbor exchange interaction in this structure,  $J_{3a}$  and  $J_{3b}$ <sup>32-34</sup>. Generally, in the cubic pyrochlore structures  $J_{3b} \ll J_{3a}$ . Therefore,  $J_{3b}$  is approximated 0<sup>32-34</sup>.

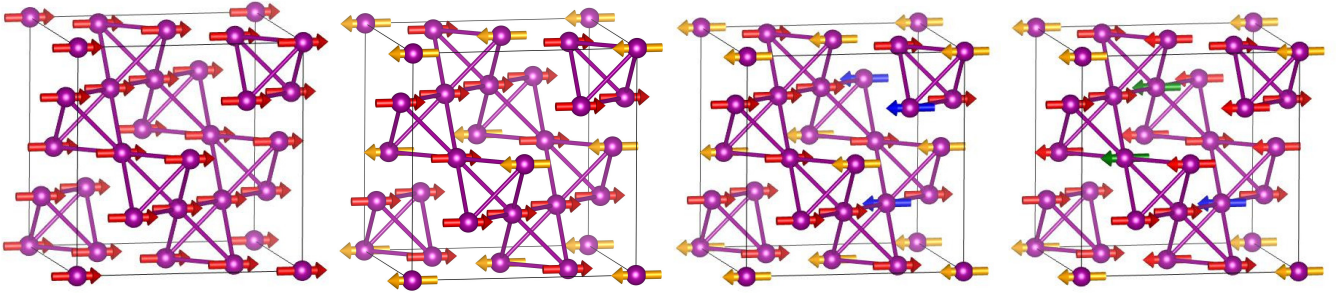


FIG. 2: (Color online) Different collinear spin configurations for calculation Heisenberg couplings. The purple spheres denote  $\text{Mn}^{2+}$ . The arrows indicate the direction of the spins for each atom. From left to right, the colors of some of the spins are selected differently to distinguish between different configurations. The ferromagnetic configuration has been chosen as the reference to calculate the total energy difference of the various configurations. In this paper, 10 different spin configurations have been used to make sure that the  $J_1$  converges with respect to the number of configurations.

The nearest neighbor coupling is important for  $B$  and anisotropic terms such as Dzyaloshinskii-Moriya coupling ( $D$ ) and single-ion anisotropy strength ( $\Delta$ ). Therefore, the primitive cell (22 atoms) with  $6 \times 6 \times 6$  optimized Monkhorst-Pack k-point mesh must be regarded. The strength of  $B$  can be determined via the total energy of noncollinear spin configurations in the absence of spin-orbit coupling (GGA+ $U$ ). In this case, if one starts from the all-in/all-out spin configuration (where all spins are oriented towards in/out center of tetrahedra) and if one rotates the spins so that  $\vec{S}_1 + \vec{S}_2 + \vec{S}_3 + \vec{S}_4 = 0$ , it can be shown that Heisenberg term is degenerated<sup>34</sup>. The total energy difference of different noncollinear spin configurations can be attributed to  $B$ <sup>34</sup>. With the uniform rotation of magnetic moments in the absence of SOC, the isotropic terms of the spin Hamiltonian are degenerated. By considering the spin-orbit coupling (GGA+ $U$ +SOC), the total energy difference of the various noncollinear spin configurations is entirely attributed to  $D$  provided that the SIA is negligible<sup>34</sup>. Given that  $\text{Mn}^{+2}$  ends in  $3d^5$ , it is expected that SIA has a very small contribution. To calculate this term, one has to examine two different noncollinear spin configurations. In the first spin configuration, one magnetic moment points outward from the center of the tetrahedra. The other three moments point inward toward the center of the tetrahedra. For the second spin configuration, the magnetic moments of the first configuration rotate about  $120^\circ$  around the  $Z$  axis. It can be demonstrated that for these two spin configurations in the absence of SOC, isotropic terms do not change. In the presence of SOC, the  $D$  remains unchanged and the total energy difference between these two spin configurations is entirely attributed to  $\Delta$ <sup>35</sup>. The derivation of Eq. (1) has been done by the full-potential linearized augmented plane wave (FPLAW) method as implemented in the FLEUR<sup>36</sup> code. For the exchange-correlation energy, I employ the Perdew Burke Ernzerhof parametrization of the generalized gradient approximation (GGA)<sup>37</sup>. The GGA+ $U$  approximation<sup>38</sup> is used to account for the on-site Coulomb interaction for  $3d$  orbitals of Mn atoms. The optimized cut-off of wave function expansion in the

interstitial region is set to  $k_{\text{max}} = 4.2 \text{ a.u.}^{-1}$ . The muffin-tin radius of Na, Sr, Mn and F atoms are set to 2.6, 2.8, 2.3 and 1.4 a.u., respectively. To increase the accuracy of the calculations, I have considered the  $3s$  and  $3p$  orbitals of the Mn as semicore electrons (FLAPW+LO).

The effective  $U$  parameter ( $U_{\text{eff}} = U - J_{\text{H}}$ ), where  $U$  and  $J_{\text{H}}$  are screened on-site Coulomb and Hund exchange interactions, is calculated by the Density Functional Perturbation Theory (DFPT)<sup>39</sup> using the Quantum-Espresso (QE) code (employing the plane waves basis set)<sup>40,41</sup>. The optimized 40 Ry and 400 Ry cutoff have been considered for expanding wavefunction and charge density in plane wave, respectively. The approximation electron-ion interactions have been controlled through GBRV ultra-soft pseudo-potential<sup>42</sup>. In order to investigate the microscopic strength of  $\delta J$  within DFT, one considers a conventional unitcell with 88 atoms. For this unitcell, one can define 97 different configurations with different A-site distributions by using the supercell program. Each of these distributions has a specific and unique symmetry. For calculations of the total energy and  $J$  parameter for each configuration, QE code has been used in GGA+ $U$  approach.

To capture the critical properties and low-temperature spacial spin arrangement of  $\text{NaSrMn}_2\text{F}_7$ , one performs MC simulation. The effect of charge disorder has been regarded in this simulation. Since SG materials have multiple local minimums in their energy landscape, reaching the global minimum especially at low-temperature is not possible. To tackle this problem, the replica exchange method<sup>43</sup> should be employed as implemented in the ES-pinS package<sup>44</sup>. The Gaussian distribution has been considered the particular choice of disorder. In the replica exchange algorithm, the high-temperature configurations are swapped for the low-temperature configurations so that the system reaches thermal equilibrium. The condition for the system to reach equilibrium is that the MC steps should be sufficiently selected so that, first, the temperature behavior of the specific heat and energy of the system is smooth and, second, the position of the specific heat peak changes slightly by changing the seed and

TABLE I: Calculated Heisenberg couplings up to third neighbors and  $D$  for different  $U_{\text{eff}}$  parameters. Negative and positive value denotes anti-ferromagnetic and ferromagnetic exchange interaction, respectively. Also, One can see calculated  $\theta_{\text{CW}}$  by MC simulations. To account the effect of random A-site occupations, one can regard  $\delta J = 0.13$  meV as a weak bond disorder. It should be noted that I consider 200-300 K as temperature range for calculation of  $\theta_{\text{CW}}$  similar to experimental range<sup>5</sup>.

$U_{\text{eff}}$ (eV)	$J_1$ (meV)	$J_2$ (meV)	$J_3$ (meV)	$D$ (meV)	$\theta_{\text{CW}}$ (K)
0.00	-8.37	-0.06	-0.02	0.100	-247.88
2.58	-4.12	-0.02	-0.02	0.010	-107.81
3.30	-3.46	-0.01	-0.02	0.005	-89.19
3.58	-3.22	-0.01	-0.02	0.002	-79.90
4.58	-2.53	-0.01	-0.02	-0.002	-64.05
EXP					-89.70 <sup>5</sup>

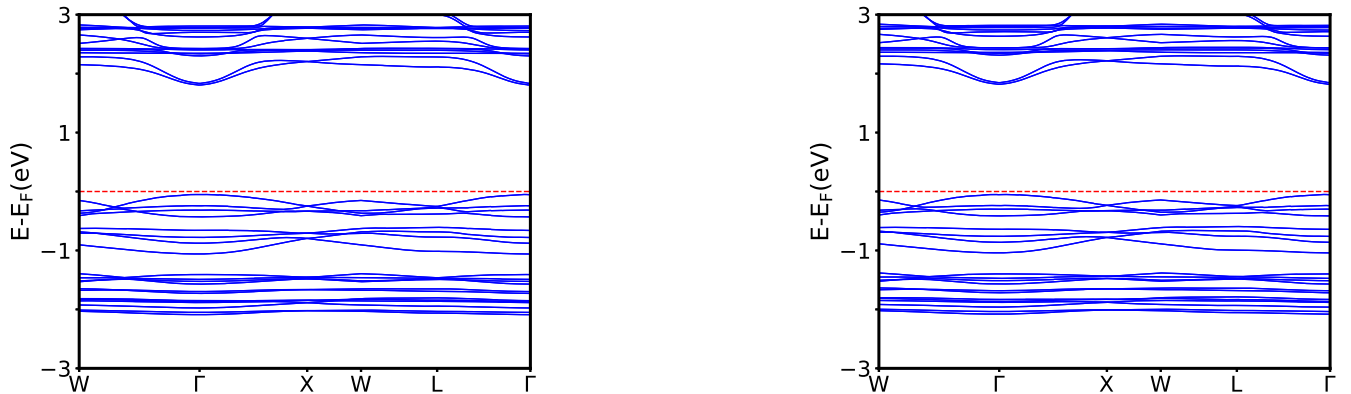


FIG. 3: (Color online) Obtained the band structure of NaSrMn<sub>2</sub>F<sub>7</sub> in **(Left)**GGA and **(Right)**GGA+SOC approaches, respectively. The Fermi energy is set to zero. The all-in/all-out magnetic configuration (noncollinear spin texture) has been considered for these calculations. The figures exhibit that the SOC has ignorable effect on energy bands near the Fermi level.

third, the acceptance ratio of MC steps at each temperature reaches at least to 65 percent. The different linear size of the simulation cell ( $L=8, 10, 12$ ) is used to ensure the presence of phase transition. In this way, there are  $N \times L^3$  spins in the three-dimensional lattice where  $N$  is the number of spins ( $N=4$  for one tetrahedron). For MC calculations, when  $\delta J$  is considered, the calculations are performed for ten different starting points (different seeds) and then the final result is expressed as the average of them.  $2 \times 10^6$  MC steps per spin at each temperature are performed for the thermal equilibrium and data collection, respectively. To reduce the correlation between the successive data, measurements are done after skipping every 10 MC steps.

### III. RESULTS AND DISCUSSION

The quantitative derivation spin Hamiltonian (Eq. (1)) is effective to explain or predict the magnetic properties of this pyrochlore. This information can answer the fundamental question about how a novel ground state emerges. The results of calculations of different spin Hamiltonian terms for different Hubbard parameters are given in Table. I. Although the obtained band struc-

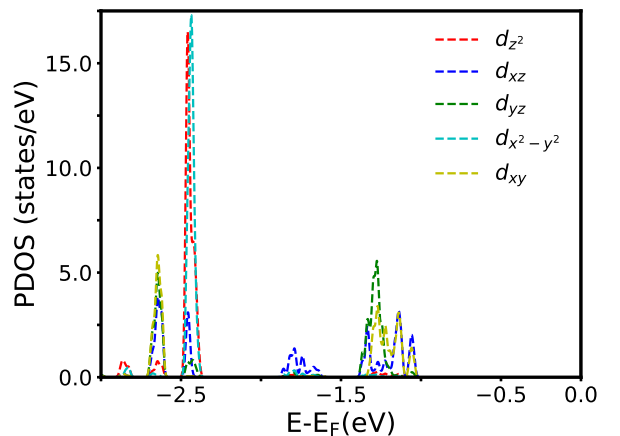


FIG. 4: (Color online) PDOS calculated for AFM-ordered NaSrMn<sub>2</sub>F<sub>7</sub> using the GGA functional. It illustrates the local 3d DOS of a single Mn atom for majority spins. The obtained Lowdin Charge analysis indicates that the majority spin levels are fully occupied and minority spin levels are negligibly occupied. That's why the 3d DOS for majority spins has not been exhibited. It should be noted that this calculation has been done by using QE code<sup>40,41</sup>.

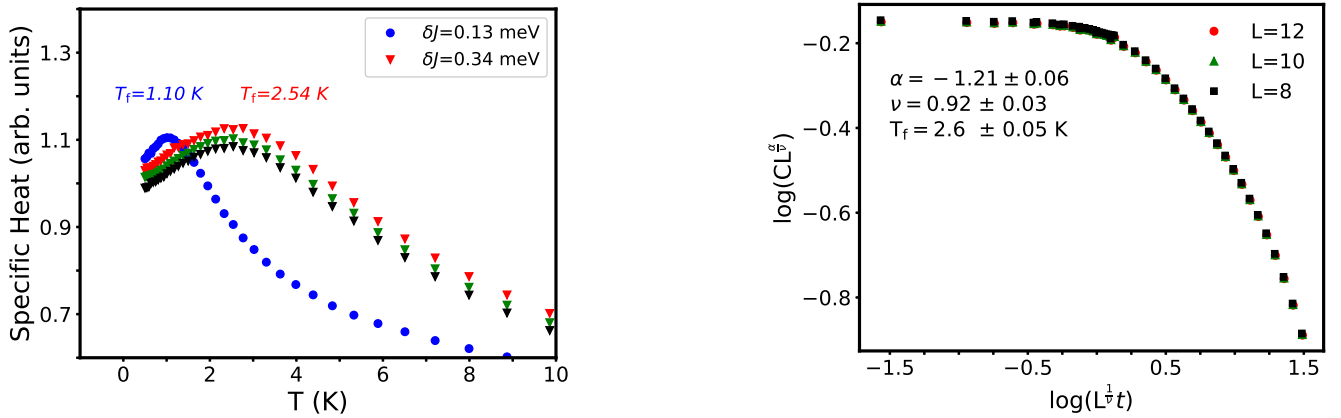


FIG. 5: (Color online) **(Left)** The calculated magnetic specific heat for different  $\delta J$  values. The freezing temperature is similar to the experimental value for  $\delta J = 0.34$  meV. A broad anomaly can be seen just for  $\delta J = 0.34$  meV which suggests the absence of long-range magnetic ordering. For  $\delta J = 0.34$  meV, the red, green and black color denotes  $L=12$ ,  $L=10$  and  $L=8$ , respectively. Changing the peak of specific heat for different sizes of the simulation cell ( $L=8, 10, 12$ ) indicates finite-size scaling which supports the value of  $T_f$ . The temperature of the peak has been considered as  $T_f$ . **(right)** The data collapsing of different lattice sizes of specific heat by using finite-size scaling theory to obtain  $T_f$  and relevant critical exponents.

ture (Fig. 3) suggests that the material is an insulator in the GGA approach, one needs to describe accurately the electron-electron Coulomb correlation due to the 3d orbital of the Mn atom. Therefore, one should apply the Hubbard potential to 3d electrons as an on-site Coulomb interaction. Based on the *ab initio* calculations (DFPT method), the effective Hubbard parameter  $U_{\text{eff}}$  obtains 4.58 eV for this system. In this paper, I have considered  $J_H \sim 1.0$  eV as it is suggested for 3d materials<sup>45,46</sup>. To ensure the exact value of  $U_{\text{eff}}$ ,  $\theta_{\text{CW}}$  obtained from the MC simulation can be compared with the experimental value. Since the  $\theta_{\text{CW}}$  is strongly dependent on  $J_1$  and  $J_1$  is strongly dependent to  $U_{\text{eff}}$ , one can control  $\theta_{\text{CW}}$  value by increasing or decreasing the Hubbard parameter. As shown in Table. I, I have started from  $U_{\text{eff}} = 4.58$  eV and decreased it until the obtained  $\theta_{\text{CW}}$  is equal to the experimental value. In this way, the optimum  $U_{\text{eff}}$  is 3.30 eV.

According to the chemical valence of different atoms in  $\text{NaSrMn}_2\text{F}_7$  compound, one expects that Na, Sr, Mn and F are in the +1, +2, +2 and -1 oxidation states, respectively. Therefore, the external shell of  $\text{Mn}^{+2}$  is  $3d^5$  and Hund's rule predicts a spin  $S=5/2$ , and thereby a magnetic moment  $5 \mu_B$  for it. The DFT calculations obtain  $4.8 \mu_B$ , not far from the native ionic picture. With this simple picture, one expects the quantum angular momentum of Mn to be zero and the magnetization of this compound originated only from the spin part. The DFT calculations give some residual magnetization  $0.024 \mu_B$ ,  $0.0008 \mu_B$  and  $0.0005 \mu_B$  for F, Sr and Na atoms, respectively.

In order to ensure that the bond disorder does not affect the crystal field and its consequence on higher order exchange interactions, one has to calculate other important and effective exchange couplings. The DFT calculations give those other exchange parameters such as  $B$ ,

$D$  and  $\Delta$  are 3 to 4 times smaller than the  $J_1$ . As a result, these interactions are negligible and do not play a significant role in determining the magnetic properties of the ground state. The antisymmetric exchange interactions (DMI and SIA) are strongly dependent on the orbital moment of the magnetic ion. Experimental measurements<sup>5</sup> show that the Mn orbital moment has a very small role in the effective orbital of this material. The  $0.0001 \mu_B$  obtains as the orbital moment of each Mn ion from *ab initio* calculations (GGA+ $U$ +SOC), which is a very small amount. It can be concluded that antisymmetric exchange interactions in this material are ignorable. In addition, Fig. 3 compares band structures for noncollinear (all-in/all-out) magnetic configuration with and without SOC. As can be seen, the effect of the SOC on the energy bands is very small, especially near the Fermi level. Therefore, SOC effect in this material is very weak and as a result. The calculations of spin-projected DOS (PDOS) and Lowdin charge analysis for an Mn atom confirm that SOC effect is negligible (Fig. 4). According to the Lowdin charge analysis, the total charge for majority and minority spin levels are  $d_{z^2}=0.9973$ ,  $d_{xz}=0.9905$ ,  $d_{yz}=0.9909$ ,  $d_{x^2-y^2}=0.9973$ ,  $d_{xy}=0.9927$  and  $d_{z^2}=0.0348$ ,  $d_{xz}=0.0723$ ,  $d_{yz}=0.0707$ ,  $d_{x^2-y^2}=0.0358$ ,  $d_{xy}=0.0723$ , respectively. Therefore, the majority spin levels are fully occupied and minority spin levels are negligibly occupied. It can be concluded that the orbital moment is quenched in this material.

The exchange parameters of the second ( $J_2$ ) and third ( $J_3$ ) nearest neighbors are very small. Thus, A-site random occupation only changes  $J_1$ . One can estimate this weak bond disorder by using  $\delta J = \sqrt{\frac{3}{8}} k_B T_f$ <sup>47</sup>. Since the experimental value of the freezing temperature is  $2.5 \text{ K}$ <sup>5</sup>,  $\delta J$  is equal to 0.13 meV. In the following, I perform MC simulations to obtain *ab initio* freezing temperature by

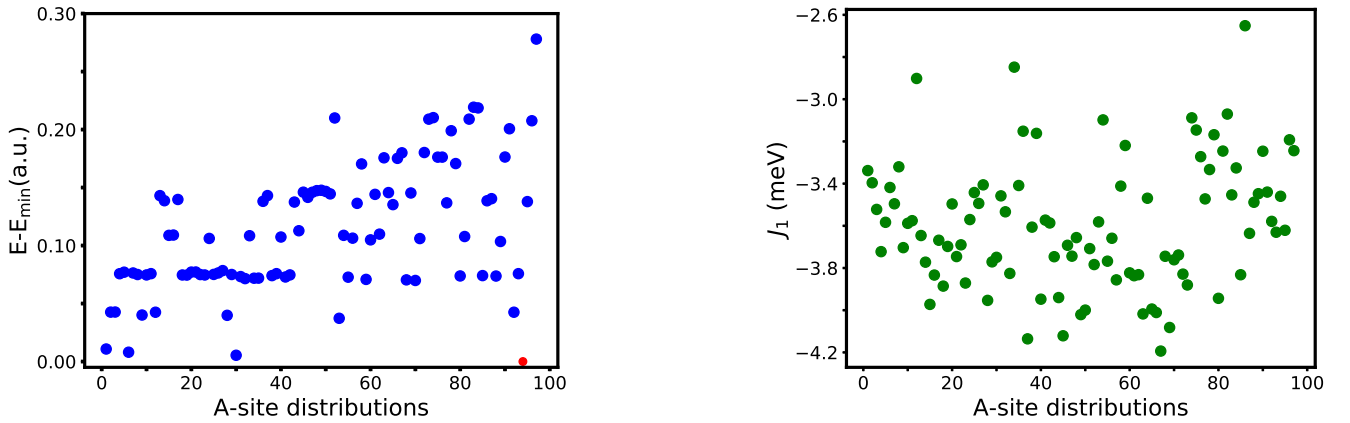


FIG. 6: (Color online) **(Left)** *Ab-initio* calculations of total energy for different A-site distributions in GGA+ $U$  approach. The purple circle which has minimum total energy is related to homogeneous distribution in which Na and Sr occupy A-site tetrahedral with two by two ratios. The total energy of homogeneous distribution has been considered as  $E_{\min}$ . **(right)** *Ab-initio* calculations of  $J_1$  for different A-site distributions in GGA+ $U$  approach. According to definition of standard deviation, one can obtain  $\delta J=0.31$  meV.

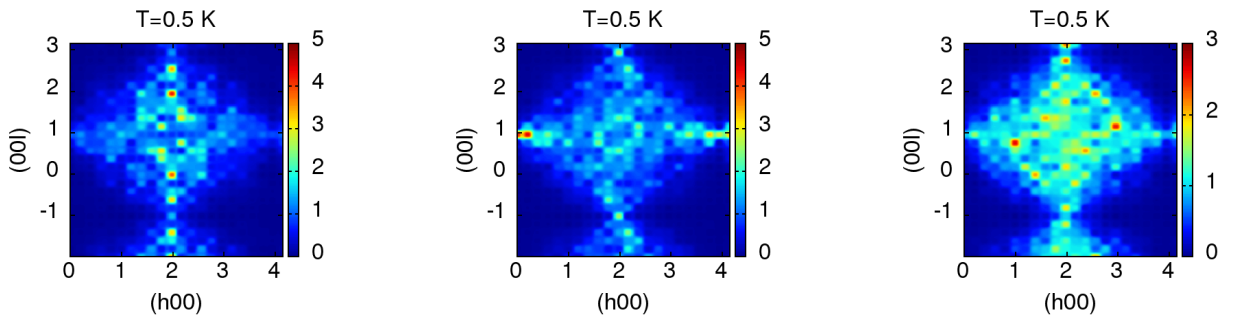


FIG. 7: (Color online) The  $(h0l)$  planes density plot of elastic neutron scattering structure function obtained by MC simulation at  $T=0.5$  K. The change in the scattering pattern indicates change in magnitude and intensity of the exchange interaction which is necessary to form the SG state.

using Eq. 1 for optimum  $U_{\text{eff}}$ . In order to account for the effect of A-site random occupation on MC simulation, the calculations are performed taking into account  $\delta J$ . Fig. 5 illustrates the temperature behavior of specific heat of the sample. The peak of specific heat has been regarded as  $T_f$ . For  $\delta J=0.13$  meV,  $T_f$  obtains 1.17 K. One increases the  $\delta J$  to reach the experimental  $T_f$ . The calculations show that the *ab initio* freezing temperature can be reached at 2.5 K for  $\delta J=0.34$  meV. By decreasing the amount of  $\delta J$ , the freezing temperature decreases so that for  $\delta J=0$ , no phase transition is observed up to 0.5 K. In order to show how much the freezing temperature ( $T_f$ ) depends on the strength of the  $\delta J$ , the MC simulations are repeated for the case where the magnitude of the  $\delta J = \sqrt{\frac{3}{8}}k_B T_f = 0.13$  meV is kept constant and the value of  $J_1 = -3.46$  meV is increased. The results of my calculations exhibit that the value of  $T_f$  has very tiny changes from 1.17 K even for  $J_1 = -4.58$  meV and it reaches  $\sim 2$  K for  $J_1 = -50$  meV. Therefore, one can say that the  $\delta J$  acts as a small perturbation and must account for the

system SG phase transition at low-temperature by eliminating the degeneracy of the ground state<sup>47</sup>. One of the remarkable features of SG materials is a broad anomaly in the specific heat data around freezing temperature. Such behavior is observed for  $\delta J=0.34$  meV.

Another question comes from how one can define the  $T_f$ . To answer this question, one uses the finite-size scaling theory<sup>48,49</sup>. The singular part of the specific heat is given by

$$c(t, L) \sim L^{\alpha/\nu} \mathcal{C}(tL^{1/\nu}) \quad (2)$$

where  $t = \frac{T_f - T}{T_f}$  is the reduced temperature and  $L$  is linear lattice size. Finite-size scaling of  $\alpha$  is shown in Fig. 5. This figure clearly shows the data collapse of the different lattice sizes ( $L=8, 10, 12$ ) by choosing  $\alpha = -1.21 \pm 0.06$ ,  $\nu = 0.92 \pm 0.03$  and  $T_f = 2.6 \pm 0.05$  K. This result shows that the estimation of  $T_f$  by changing  $\delta J$  has good accuracy. The negative value for  $\alpha$  has been reported for other SG and SG-frustrated materials<sup>50-54</sup>.

To prove the obtained  $\delta J=0.34$  meV, one calculates

the microscopic strength of  $\delta J$  within DFT. Since Na and Sr occupy A-site fully randomly with equal parts, one defines different 97 geometries with different Na/Sr distributions. Fig. 6 shows how different 97 configurations are arranged in terms of total energy. According to Fig. 6, one distribution has the lowest total energy. It can be called homogeneous distribution because Na-Sr occupies A-site in such a way that in each A-site tetrahedral, there are two Sr and two Na. Therefore, one can only make a primitive cell with 22 atoms for only this distribution.

To determine the magnetic order of the system below  $T_f$ , one calculates the elastic neutron scattering structure function ( $S(\vec{q})$ ) for different seeds.  $S(\vec{q})$  is given by<sup>12</sup>:

$$S(\vec{q}) = \sum_{i,j} \langle (\vec{S}_i - \frac{\vec{S}_i \cdot \vec{q}}{\vec{q} \cdot \vec{q}} \vec{q}) \cdot (\vec{S}_j - \frac{\vec{S}_j \cdot \vec{q}}{\vec{q} \cdot \vec{q}} \vec{q}) \rangle \exp[i\vec{q} \cdot (\vec{R}_i - \vec{R}_j)]. \quad (3)$$

in which  $\vec{R}_i$  is the position of each of the four spins in the tetrahedron unit cell  $i = 1 \dots N_{\text{cell}}$ ,  $\vec{q}$  is the wave vector and  $\vec{S}_i$  denotes the direction of each spin at the tetrahedron. Fig. 7 show the density plots of  $S(\vec{q})$  for different seeds at  $T=0.5$  K in (h0l) planes. According to Fig. 7,  $S(\vec{q})$  has different patterns. Therefore, one concludes that the ground state below  $T_f$  has an SG order. Because the different scattering patterns show that the distribution of  $J$  differs in terms of strength and magnitude. Random exchange interaction is one of the requirements for the emergence of the glass spin ground state.

Another feature of SG materials is that they undergo a second-order phase transition. For MC simulations, the order of transition is obtained by the Binder fourth energy cumulant given by<sup>55</sup>:

$$U(T) = 1 - \frac{1}{3} \frac{\langle E^4 \rangle}{\langle E^2 \rangle^2}, \quad (4)$$

in which  $E$  is the total energy of the system which can be calculated by MC. The  $L$  dependence of minimum of  $U(T)$  at critical temperature is given by<sup>55</sup>:

$$U_{\text{min}}(L) = U^* + AL^{-3} + BL^{-6} + O(L^{-9}) \quad (5)$$

Fig. 8 illustrates the scaling of the Binder cumulant minimum versus  $L^{-3}$ . For  $U^* < \frac{2}{3}$  and  $U^* = \frac{2}{3}$ , the order of phase transition is first and second-order, respectively<sup>55</sup>. The obtained  $U^* = 0.666663(6)$  shows that this system goes to the low-temperature spin-glass ground state with second-order phase transition.

#### IV. CONCLUSION

In summary, a spin Hamiltonian for spin-glass pyrochlore  $\text{NaSrMn}_2\text{F}_7$  by using DFT calculations obtained. Spin Hamilton included isotropic and anisotropic

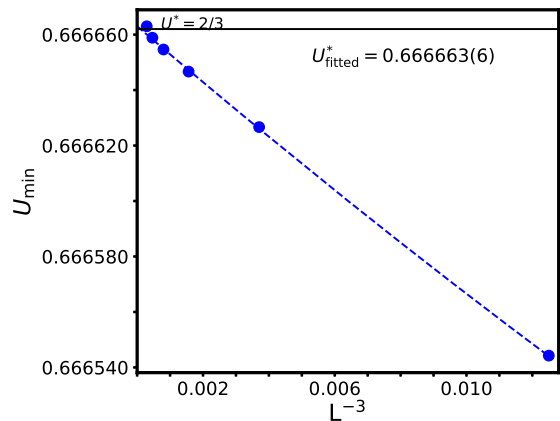


FIG. 8: (Color online) The scaling behavior of the minimum of Binder fourth energy cumulant  $U_{\text{min}}$  versus  $L^{-3}$ . The dashed lines are obtained by fitting Eq. (5) to the data. We use the MC simulation data on the lattices with  $L = 4, 6, 8, 10, 12$  and  $14$ .

terms such as Heisenberg coupling up to third neighbors, nearest neighbor bi-quadratic, Dzyaloshinskii-Moriya and single-ion anisotropy. Since the Hubbard parameter played a decisive role in describing the electron-electron correlation and consequently the magnetic properties, this value was determined via the DFPT method. Then, I reduced it to such an extent that the  $\theta_{\text{CW}}$  obtained from the MC simulations equaled to the experimental  $\theta_{\text{CW}}$ . The DFT calculations showed that only  $J_1$  (as nearest neighbor Heisenberg exchange) is the most important factor in determining the magnetic properties of this material. In the following, the specific heat temperature behavior was calculated by using the obtained spin Hamiltonian via MC simulations. Since Na-Sr random occupancy on A-site causes weak bond disorder ( $\delta J$ ),  $\delta J$  was increased to such an extent that the calculated freezing temperature equals the experimental freezing temperature. To prove this claim, the microscopic calculation of  $\delta J$  within DFT was done. To this end,  $J_1$  distribution was calculated for different Na/Sr distributions. The obtained result showed that  $\delta J$  from DFT calculations was in good agreement with calculated  $\delta J$  by using the Monte Carlo simulations. I found that  $\delta J$  behaves like a perturbation so that it is responsible for spin-glass phase transition at low-temperatures. To prove the ground state below critical temperature is spin-glass, I calculated the elastic neutron scattering structure function ( $S(\vec{q})$ ) in (h,0,l) planes for different seeds. I conclude that the distribution of  $J$  differs in terms of strength and magnitude. By using finite-size scaling theory, I found that the  $\alpha$  as a specific heat critical exponent was negative which is the feature of spin-glass systems. As a suggestion, experimental measurements such as inelastic neutron scattering can help us to understand the nature of fluctuations at low-temperatures and their effect on electron-electron correlation.

## Acknowledgments

Jülich Supercomputing Centre (JSC) is gratefully acknowledged by authors as the provider of needed comput-

ing facilities. The guidelines provided by Peter Kratzer, Marjana Ležaić and Mojaba Alaei are highly valued and appreciated.

- 
- \* Electronic address: [mo.amirabbasi@gmail.com](mailto:mo.amirabbasi@gmail.com)
- <sup>1</sup> J. A. Mydosh, *Spin glasses: an experimental introduction* (CRC Press, 1993).
  - <sup>2</sup> K. Binder and A. P. Young, *Rev. Mod. Phys.* **58**, 801 (1986).
  - <sup>3</sup> T. Taniguchi, T. Munenaka, and H. Sato, in *Journal of Physics: Conference Series*, Vol. 145 (IOP Publishing, 2009) p. 012017.
  - <sup>4</sup> H. Shintani and H. Tanaka, *Nature Physics* **2**, 200 (2006).
  - <sup>5</sup> M. Sanders, J. Krizan, K. Plumb, T. McQueen, and R. Cava, *Journal of Physics: Condensed Matter* **29**, 045801 (2016).
  - <sup>6</sup> H. Kawamura and T. Taniguchi, *Chapter 1 - Spin Glasses*, edited by K. Buschow, *Handbook of Magnetic Materials*, Vol. 24 (Elsevier, 2015) pp. 1 – 137.
  - <sup>7</sup> E. Vincent and V. Dupuis, in *Frustrated Materials and Ferromagnetic Glasses* (Springer, 2018) pp. 31–56.
  - <sup>8</sup> K. Mitsumoto, C. Hotta, and H. Yoshino, *Phys. Rev. Lett.* **124**, 087201 (2020).
  - <sup>9</sup> H. Shinaoka, Y. Tomita, and Y. Motome, *Phys. Rev. Lett.* **107**, 047204 (2011).
  - <sup>10</sup> M. Subramanian, G. Aravamudan, and G. Subba Rao, *Progress in Solid State Chemistry* **15**, 55 (1983).
  - <sup>11</sup> J. S. Gardner, M. J. P. Gingras, and J. E. Greedan, *Rev. Mod. Phys.* **82**, 53 (2010).
  - <sup>12</sup> C. Lacroix, P. Mendels, and F. Mila, *Introduction to frustrated magnetism: materials, experiments, theory*, Vol. 164 (Springer Science & Business Media, 2011).
  - <sup>13</sup> D. Reig-i Plessis and A. M. Hallas, *Phys. Rev. Materials* **5**, 030301 (2021).
  - <sup>14</sup> M. J. Harris, S. T. Bramwell, D. F. McMorrow, T. Zeiske, and K. W. Godfrey, *Phys. Rev. Lett.* **79**, 2554 (1997).
  - <sup>15</sup> D. Slobinsky, L. Pili, G. Baglietto, S. Grigera, and R. Borzi, *Communications Physics* **4**, 1 (2021).
  - <sup>16</sup> R. Moessner and S. L. Sondhi, *Physical Review B* **68**, 064411 (2003).
  - <sup>17</sup> F. P. Marilton, Z. Zhang, Y. Zhang, T. E. Proffen, C. D. Ling, and B. J. Kennedy, *Chemistry of Materials* (2021), [10.1021/acs.chemmater.0c04515](https://doi.org/10.1021/acs.chemmater.0c04515).
  - <sup>18</sup> D. Yahne, D. Pereira, L. Jaubert, L. Sanjeewa, M. Powell, J. Kolis, G. Xu, M. Enjalran, M. Gingras, and K. Ross, arXiv preprint [arXiv:2101.08361](https://arxiv.org/abs/2101.08361) (2021).
  - <sup>19</sup> Y. Shi, C. Nisoli, and G.-W. Chern, *Applied Physics Letters* **118**, 122407 (2021).
  - <sup>20</sup> T. Fennell, P. Deen, A. Wildes, K. Schmalzl, D. Prabhakaran, A. Boothroyd, R. Aldus, D. McMorrow, and S. Bramwell, *Science* **326**, 415 (2009).
  - <sup>21</sup> S. T. Bramwell and M. J. Gingras, *Science* **294**, 1495 (2001).
  - <sup>22</sup> J. W. Krizan and R. J. Cava, *Phys. Rev. B* **89**, 214401 (2014).
  - <sup>23</sup> J. W. Krizan and R. J. Cava, *Phys. Rev. B* **92**, 014406 (2015).
  - <sup>24</sup> J. Krizan and R. J. Cava, *Journal of Physics: Condensed Matter* **27**, 296002 (2015).
  - <sup>25</sup> A. Andreev, J. T. Chalker, T. E. Saunders, and D. Sherrington, *Phys. Rev. B* **81**, 014406 (2010).
  - <sup>26</sup> A. Alexandradinata, N. Armitage, A. Baydin, W. Bi, Y. Cao, H. J. Changlani, E. Chertkov, E. H. Neto, L. Delacretaz, I. E. Baghari, *et al.*, arXiv preprint [arXiv:2010.00584](https://arxiv.org/abs/2010.00584) (2020).
  - <sup>27</sup> R. Moessner and J. T. Chalker, *Phys. Rev. Lett.* **80**, 2929 (1998).
  - <sup>28</sup> J. Yang, A. Samarakoon, S. Dissanayake, H. Ueda, I. Klich, K. Iida, D. Pajeroski, N. P. Butch, Q. Huang, J. R. Copley, *et al.*, *Proceedings of the National Academy of Sciences* **112**, 11519 (2015).
  - <sup>29</sup> O. Cepas and B. Canals, *Physical Review B* **86**, 024434 (2012).
  - <sup>30</sup> T. Moriya, *Phys. Rev.* **120**, 91 (1960).
  - <sup>31</sup> M. Elhajal, B. Canals, R. Sunyer, and C. Lacroix, *Phys. Rev. B* **71**, 094420 (2005).
  - <sup>32</sup> B. J. Kennedy, *Physica B: Condensed Matter* **241-243**, 303 (1997), proceedings of the International Conference on Neutron Scattering.
  - <sup>33</sup> A. S. Wills, M. E. Zhitomirsky, B. Canals, J. P. Sanchez, P. Bonville, P. D. de Réotier, and A. Yaouanc, *Journal of Physics: Condensed Matter* **18**, L37 (2006).
  - <sup>34</sup> A. Sadeghi, M. Alaei, F. Shahbazi, and M. J. P. Gingras, *Phys. Rev. B* **91**, 140407 (2015).
  - <sup>35</sup> H. J. Xiang, E. J. Kan, M.-H. Whangbo, C. Lee, S.-H. Wei, and X. G. Gong, *Phys. Rev. B* **83**, 174402 (2011).
  - <sup>36</sup> FLEURgroup, “<http://www.flapw.de/>,” .
  - <sup>37</sup> J. P. Perdew, K. Burke, and M. Ernzerhof, *Phys. Rev. Lett.* **77**, 3865 (1996).
  - <sup>38</sup> M. Cococcioni and S. de Gironcoli, *Phys. Rev. B* **71**, 035105 (2005).
  - <sup>39</sup> I. Timrov, N. Marzari, and M. Cococcioni, *Phys. Rev. B* **98**, 085127 (2018).
  - <sup>40</sup> P. Giannozzi, S. Baroni, N. Bonini, M. Calandra, R. Car, C. Cavazzoni, D. Ceresoli, G. L. Chiarotti, M. Cococcioni, I. Dabo, A. D. Corso, S. de Gironcoli, S. Fabris, G. Fratesi, R. Gebauer, U. Gerstmann, C. Gougoussis, A. Kokalj, M. Lazzeri, L. Martin-Samos, N. Marzari, F. Mauri, R. Mazzarello, S. Paolini, A. Pasquarello, L. Paulatto, C. Sbraccia, S. Scandolo, G. Sclauzero, A. P. Seitsonen, A. Smogunov, P. Umari, and R. M. Wentzcovitch, *Journal of Physics: Condensed Matter* **21**, 395502 (2009).
  - <sup>41</sup> P. Giannozzi, O. Andreussi, T. Brumme, O. Bunau, M. B. Nardelli, M. Calandra, R. Car, C. Cavazzoni, D. Ceresoli, M. Cococcioni, N. Colonna, I. Carnimeo, A. D. Corso, S. de Gironcoli, P. Delugas, R. A. DiStasio, A. Ferretti, A. Floris, G. Fratesi, G. Fugallo, R. Gebauer, U. Gerstmann, F. Giustino, T. Gorni, J. Jia, M. Kawamura, H.-Y. Ko, A. Kokalj, E. Küçükbenli, M. Lazzeri, M. Marsili, N. Marzari, F. Mauri, N. L. Nguyen, H.-V. Nguyen, A. O. de-la Roza, L. Paulatto, S. Poncè, D. Rocca, R. Sabatini, B. Santra, M. Schlipf, A. P. Seitsonen, A. Smogunov, I. Timrov, T. Thonhauser, P. Umari, N. Vast, X. Wu, and S. Baroni, *Journal of Physics: Condensed Matter* **29**,

- 465901 (2017).
- <sup>42</sup> K. F. Garrity, J. W. Bennett, K. M. Rabe, and D. Vanderbilt, *Computational Materials Science* **81**, 446 (2014).
- <sup>43</sup> K. Hukushima and K. Nemoto, *Journal of the Physical Society of Japan* **65**, 1604 (1996).
- <sup>44</sup> N. Rezaei, M. Alaei, and H. Akbarzadeh, *Computational Materials Science* **202**, 110947 (2022).
- <sup>45</sup> J. M. D. Coey, M. Venkatesan, and H. Xu, "Introduction to magnetic oxides," in *Functional Metal Oxides* (John Wiley and Sons, Ltd, 2013) Chap. 1, pp. 1–49.
- <sup>46</sup> L. Vaugier, H. Jiang, and S. Biermann, *Phys. Rev. B* **86**, 165105 (2012).
- <sup>47</sup> T. Saunders and J. Chalker, *Physical review letters* **98**, 157201 (2007).
- <sup>48</sup> M. E. Fisher and M. N. Barber, *Physical review letters* **28**, 1516 (1972).
- <sup>49</sup> D. P. Landau, *Phys. Rev. B* **13**, 2997 (1976).
- <sup>50</sup> K. Gunnarsson, P. Svedlindh, P. Nordblad, L. Lundgren, H. Aruga, and A. Ito, *Phys. Rev. B* **43**, 8199 (1991).
- <sup>51</sup> Y. Yeshurun, M. B. Salamon, K. V. Rao, and H. S. Chen, *Phys. Rev. Lett.* **45**, 1366 (1980).
- <sup>52</sup> M. J. P. Gingras, C. V. Stager, N. P. Raju, B. D. Gaulin, and J. E. Greedan, *Phys. Rev. Lett.* **78**, 947 (1997).
- <sup>53</sup> A. Andreev, J. T. Chalker, T. E. Saunders, and D. Sherrington, *Phys. Rev. B* **81**, 014406 (2010).
- <sup>54</sup> G. F. Hawkins, R. L. Thomas, and A. M. de Graaf, *Journal of Applied Physics* **50**, 1709 (1979).
- <sup>55</sup> K. Binder, *Phys. Rev. Lett.* **47**, 693 (1981).